Hofrichter, J., Sommer, J. H., Henry, E. R., & Eaton, W. A. (1983) *Proc. Natl. Acad. Sci. U.S.A. 80*, 2235–2239.
Hofrichter, J., Henry, E. R., Sommer, J. H., Deutsch, R. D., Ikeda-Saito, M., Yonetani, T., & Eaton, W. A. (1985) *Biochemistry 24*, 2667–2679.
Lumry, R., & Rosenberg, A. (1975) in *L'eau, Et Les Systemes Biologiques* (Alfen, A., & Berteaud, A. J., Eds.) pp 53–61, Centre National de Recherche Scientifique, Paris.
Martin, J. L., Migus, A., Poyart, C., Lecarpentier, Y., Antonetti, A., & Orszag, A. (1982) *Biochem. Biophys. Res. Commun. 107*, 803–810.
Martin, J. L., Migus, A., Poyart, C., Lecarpentier, Y., Astier, R., & Antonetti, A. (1983) *Proc. Natl. Acad. Sci. U.S.A. 80*, 173–177.
Mims, M. P., Porras, A. G., Olson, J. S., Noble, R. W., & Peterson, J. A. (1983) *J. Biol. Chem. 258*, 14219–14232.
Olson, J. S., & Gibson, Q. H. (1971) *J. Biol. Chem. 246*, 5241–5253.
Olson, J. S., McKinnie, R. E., Mims, M. P., & White, D. K. (1983) *J. Am. Chem. Soc. 105*, 1522–1527.
Reynolds, A. H., & Rentzepis, P. M. (1982) *Biophys. J. 38*, 15–18.
Reynolds, A. H., Rand, S. D., & Rentzepis, P. M. (1981) *Proc. Natl. Acad. Sci. U.S.A. 78*, 2292–2296.
Schoenborn, B. P. (1967) *Nature (London) 214*, 1120–1122.
Shrager, R. I., & Hendler, R. W. (1982) *Anal. Chem. 54*, 1147–1152.
Sommer, J. H., Henry, E. R., Hofrichter, J., & Eaton, W. A. (1983) *Biophys. J. 41*, 8a.
Stetzkowski, F., Cassoly, R., & Banerjee, R. (1979) *J. Biol. Chem. 254*, 11351–11356.
Wishnia, A. (1969) *Biochemistry 8*, 5064–5074.

^{1}H NMR Study of Labile Proton Exchange in the Heme Cavity as a Probe for the Potential Ligand Entry Channel in Myoglobin†

Juliette T. J. Lecomte and Gerd N. La Mar*
Department of Chemistry, University of California, Davis, California 95616
Received March 28, 1985

ABSTRACT: The exchange rates of heme cavity histidine nitrogen-bound protons in horse and dog metcyanomyoglobins have been determined at 40 °C as a function of pH by ^{1}H NMR spectroscopy. They were compared to the results reported for the sperm whale homologue [Cutnell, J. D., La Mar, G. N., & Kong, S. B. (1981) *J. Am. Chem. Soc. 103*, 3567–3572]. The rate profiles suggest that the exchange follows EX_2-type kinetics, and the relative rate values favor a penetration model over a local unfolding model. It was found that the behavior of protons located on the proximal side of the heme is similar in the three proteins. The distal histidyl imidazole NH, however, shows a highly accelerated hydroxyl ion catalyzed rate in horse and dog myoglobins relative to that in sperm whale myoglobin. NMR spectral and relaxational characteristics of the assigned heme cavity protons indicate that the global geometry of the heme pocket is highly conserved in the ground-state structure of the three proteins. We propose a model that attributes the different distal histidine exchange behavior to the relative dynamic stability of the distal heme pocket in dog or horse myoglobin vs. sperm whale myoglobin. This model involves a dynamic equilibrium between a closed heme pocket as found in metaquomyoglobin [Takano, T. (1977) *J. Mol. Biol. 110*, 537–568] and an open pocket as found in phenylmetmyoglobin [Ringe, D., Petsko, G. A., Kerr, D. E., & Ortiz de Montellano, P. R. (1984) *Biochemistry 23*, 2–4]. The greater stabilization of the open pocket in horse and dog myoglobins relative to sperm whale myoglobin is rationalized by the substitution CD3 Arg (sperm whale) → Lys (horse, dog). This residue holds the pocket closed in sperm whale myoglobin via hydrogen bonds to both a heme propionate and Asp E3; the substituted Lys is not capable of forming both of those stabilizing interactions in dog and horse myoglobins. Our results indicate that labile proton exchange of histidine can serve as a general useful probe of the mechanism of interaction between solvent and buried side-chain sites in folded proteins.

Proteins in general, and the oxygen-binding proteins myoglobin and hemoglobin in particular, exhibit a wide range of structural fluctuations about an equilibrium structure (Gurd & Rothgeb, 1979; McCammon & Karplus, 1980; Karplus & McCammon, 1981; Debrunner & Frauenfelder, 1982; McCammon & Karplus, 1983; Woodward et al., 1982; McCammon, 1984) which is essentially that described in the X-ray studies (Perutz & Mathews, 1966; Perutz, 1976; Takano, 1977a,b; Phillips, 1980). Some of the dynamic properties that can be clearly traced to function are the side-chain motions allowing the formation of transient channels through which molecular oxygen enters and leaves the heme cavity (Perutz & Mathews, 1966; Takano, 1977a,b; Case & Karplus, 1979). While there may be several pathways for O_2 entry, a recent X-ray structure of phenyl-ligated metmyoglobin (metMb)[1] (Ringe et al., 1984) has revealed an open "door" to the heme pocket: the reported structural differences with respect to metMbH_2O involve solely the orientation of the

† This research was supported by Grants CHE-81-08766 and CHE-84-15329 from the National Science Foundation.
* Author to whom correspondence should be addressed.

[1] Abbreviations: Mb, myoglobin(s); metMb, metmyoglobin(s); metMbCN, metcyanomyoglobin(s); NMR, nuclear magnetic resonance.

0006-2960/85/0424-7388$01.50/0

distal amino acid side chains Arg 45 (CD3), His 64 (E7), and Val 68 (E11) and the heme 6-propionate group. Thus the displacement of these groups could provide one of the major "gated" passageways to the iron in other ligated or nonligated forms of the protein (Nobbs, 1966; Case & Karplus, 1979).

At ambient temperatures the chemical exchange of a labile proton buried in the protein interior results from low activation energy fluctuations of the structure that expose its site transiently to the solvent (Hvidt & Nielsen, 1966; Woodward et al., 1982). This process is usually discussed in terms of two extreme cases: the "local unfolding" model (Englander, 1975) or the "solvent penetration" model (Woodward & Hilton, 1979; Woodward et al., 1982). In the former description, a small portion of the protein interior unfolds and becomes exposed to the solvent; in the latter model, rapid structural fluctuations of small amplitude allow the entry and the diffusion of the solvent inside the protein matrix. The combined fluctuations may create transient crevices or channels, and consequently, the solvent penetration model might bear some relevance to the mode of O_2 entry in the heme pocket.

The exchange rate of an exposed labile proton, as found in a model compound or in the denatured protein, can be written as

$$\tau^{-1} = k_A[H^+]^n + k_B[OH^-]^m + k_W[H_2O] \qquad (1)$$

where k_A and k_B are the rate constants for H^+ and OH^- catalysis, respectively, and k_W is generally neglected (Woodward et al., 1982). For a buried proton, when the site exposure step—either unfolding or penetration—is not rate-limiting (EX_2 case; Hvidt & Nielsen, 1966; Woodward & Hilton, 1979), the mechanism of exchange is unaltered, but the rates are retarded by the probability of finding the site exposed; exponents n and m less than unity are interpreted as evidence for exchange in a medium different from bulk water. Thus the EX_2 mechanism can be established on the basis of the pH dependence of the exchange rates.

Proton NMR provides a powerful method for studying labile proton exchange in solution because of its potential for resolving and assigning individual sites. In the case of the paramagnetic forms of hemoproteins (La Mar, 1979), the ability to resolve signals from labile protons in the heme cavity and to assign them unambiguously on the basis of the differential paramagnetic relaxation is particularly useful: the labile proton intensity can be monitored readily to provide information about the dynamics of the heme pocket (Cutnell et al., 1981; La Mar & Krishnamoorthi, 1983). As an initial study, we reported on the assignment and behavior or four such resolved exchangeable proton resonances in sperm whale metMbCN (La Mar, 1979; Cutnell et al., 1981): the ring NHs of His F8 (proximal), His E7 (distal), and tentatively His FG3 (parallel to the heme on the proximal side; Takano, 1977a,b) and the peptide NH of His F8. The location of those protons in the heme pocket is represented in Figure 1A.

The behavior of histidine residues should be particularly informative for the mechanism of hydrogen exchange, as H^+ and OH^- catalyses involve an attack at different positions of the neutral imidazole side chain. Acid attack necessarily proceeds at the free nitrogen (N_1 for His E7 and for His FG3; Takano, 1977a,b). On the other hand, base-catalyzed exchange calls for hydroxide attack at N_3H in each case. Thus the local unfolding process, since it exposes the histidine side chain to the solvent, should accelerate both mechanisms comparably. In the case of solvent penetration, the two mechanisms may be retarded differentially depending on the position of the two sites relative to the transient channel. In this respect, histidine side chains can be compared to peptide

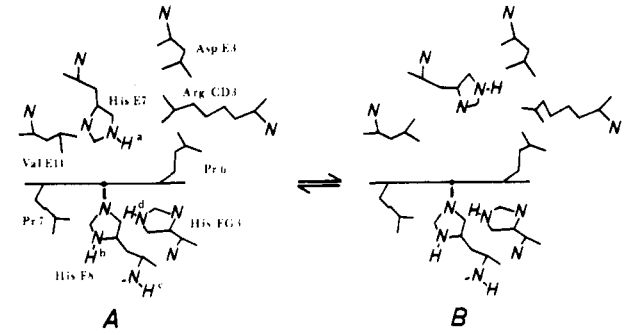

FIGURE 1: Heme environment in sperm whale myoglobin. (A) Ligand channel closed (Takano, 1977a,b); (B) ligand channel open (Ringe et al., 1984). Only the residues of interest are represented.

amide protons for which it has been shown that the site of attack depends on the nature of the catalyst—H^+ reacts with the O atom whereas OH^- acts on the NH group (Perrin & Arrhenius, 1982)—and, hence, comparison of the two rates in proteins and models can be used to infer conclusions as to the nature of the species that exposes the site to the solvent. In bovine pancreatic trypsin inhibitor, variations in acid and base rate constants have been analyzed successfully in terms of accessibility of C=O and NH groups (Tuchsen & Woodward, 1985).

In myoglobin, one histidine (F8) is attached through the N_3 atom to the heme iron; this precludes acid attack on the ring. Only base-catalyzed ring NH exchange has been observed for the coordinated histidines in a variety of heme proteins. The proton attributed to His FG3, which participates in hydrogen bonding to a heme propionate, exhibits comparable rates of acid- and base-catalyzed exchange, as expected for the free amino acid. The third conserved histidine in myoglobin, the distal His E7, exhibits primarily acid-catalyzed exchange in sperm whale metMbCN and in various derivatives thereof containing modified hemes (La Mar & Krishnamoorthi, 1983). Initially, we interpreted this altered exchange behavior in the protein solely in terms of the nature of interaction in the ground-state structure; namely, the labile ring proton of His E7 interacts with the coordinated cyanide ligand, probably via a strong hydrogen bond as originally suggested by Bretscher (1968) and observed in the X-ray and neutron diffraction data of sperm whale MbO_2 (Phillips & Schoenborn, 1981).

Whether the strongly retarded base-catalyzed exchange of a distal histidine is a property of the strength of the interaction with the coordinated ligand in the ground-state structure or whether it reflects the peculiar protein dynamics that control the pathway by which acid or base approaches these respective sites on the imidazole ring can be elucidated in a study of a variety of myoglobins for which a conserved ground-state structure can be demonstrated.

We report herein on the ^{1}H relaxation and saturation transfer NMR study of the labile protons in the heme cavity of the horse and dog skeletal metMbCN complexes and compare the data with our previous results on the sperm whale complex (Cutnell et al., 1981). We demonstrate that, in spite of highly conserved structures of the heme cavity, both horse and dog Mb exhibit a dramatically altered exchange behavior of the distal histidine residue. We attribute the effect to changes in the protein dynamics that expose transiently the distal histidine to the two exchange catalysts and show that this difference in the access of base to the heme cavity is correlated with an amino acid replacement, CD3 Arg (sperm whale) → Lys (horse, dog), near the surface of a proposed pathway for ligand access to the heme pocket in myoglobin.

Materials and Methods

Sperm whale, horse, and dog myoglobins from skeletal muscle were purchased from Sigma as salt-free, lyophilized powders and used without further purification. The solutions for NMR experiments were 1.5–2 mM in protein in either ^2H_2O, 0.2 M in NaCl, or 90% H_2O/10% ^2H_2O, 0.2 M in NaCl. The metcyano forms were prepared by addition of excess KCN, and the pH was adjusted with 0.1 M NaO^2H or ^2HCl (or 0.1 M NaOH and HCl in 90% H_2O/10% ^2H_2O). The pH of the samples was read with a Beckman Model 3550 pH meter equipped with an Ingold microcombination electrode; the values used are not corrected for isotope effect. All proton NMR spectra were recorded at 360 MHz in the FT quadrature mode on a Nicolet NT-360 NMR spectrometer over a 12-kHz bandwidth with 8192 data points.

The nonselective spin–lattice relaxation time T_1 may be used for structural elucidation in low-spin ferric myoglobin (Swift, 1973; Cutnell et al., 1981). Since the relaxation process is dominated by paramagnetic interactions mostly dipolar in nature, the ratio of distances r from the iron to two nonequivalent protons i and j can be obtained from their ratio of T_1 values (Cutnell et al., 1981) according to

$$r_i/r_j = (T_{1i}/T_{1j})^{1/6} \quad (2)$$

provided the ligand-centered contribution to T_1 can be ignored (Unger et al., 1985). Nonselective spin–lattice relaxation parameters were determined by the 180°–τ–90° inversion–recovery method (Vold et al., 1968) using a composite 180° pulse (Levitt, 1982). The H_2O line was saturated off-acquisition with the decoupler for the 90% H_2O samples.

Rates of exchange were measured by the saturation transfer method. The extent of saturation transferred from the irradiated solvent line to the exchangeable proton resonances was determined as proposed by Cutnell et al. (1981): a Redfield excitation, used for observation, is centered on the region of interest (around 21 ppm), and the pulse lengths are optimized to generate a minimal perturbation of the water line. The decoupler is applied off-acquisition either to the H_2O transition, causing complete saturation, or to an off-resonance frequency. The pair of spectra so obtained yields the needed I, the intensity observed when the solvent is saturated, and I_0, the intensity in the absence of saturation. The corresponding saturation factor $F = I/I_0$ is then determined. The rate of exchange is related to F by the formula

$$F = \rho/(\rho + \tau^{-1}) \quad (3)$$

where ρ is the intrinsic relaxation rate of the resonance whose F is evaluated. If the intrinsic relaxation time ρ^{-1} is independently known and remains constant over the pH range, the exchange rate is obtainable from

$$\tau^{-1} = \rho(1 - F)/F \quad (4)$$

In the presence of exchange, and when ρ^{-1} cannot be determined directly, the following equation yields the rate:

$$\tau^{-1} = (1 - F)\rho' \quad (5)$$

where ρ' is the effective relaxation rate of the exchanging resonance and is given by $\rho' = \rho + \tau^{-1}$. In such a case, ρ can be extracted by using

$$\rho = \rho' F \quad (6)$$

The selective spin–lattice relaxation rates necessary to analyze the saturation transfer data were determined as follows. At pH values where the lifetime τ of the labile proton is long compared to its intrinsic relaxation time ρ^{-1}, a selective saturation recovery experiment with a Redfield 2–1–4–1–2 excitation pulse sequence (Redfield et al., 1975) was performed. At pH values where ρ^{-1} and τ have comparable magnitudes, effective spin–lattice relaxation rates were obtained by selective inversion recovery with saturation of the H_2O line at all times except during acquisition (Campbell et al., 1978). All recovery data, selective and nonselective, were analyzed with a three-parameter nonlinear least-squares fit to the equation $(I_\infty - I_t)/2I_\infty = A\exp(-t/q)$, where I_∞ and I_t are the intensity at infinite time (with or without H_2O saturation depending on the experiment) and the intensity after a recovery period t, respectively. The q values correspond to the nonselective relaxation time T_1, the selective (intrinsic) relaxation time ρ^{-1}, or the effective relaxation time $\rho'^{-1} = (\rho + \tau^{-1})^{-1}$, according to the experiment type and conditions. The uncertainty is estimated at 8% on the basis of reproducibility and standard deviation of the fits.

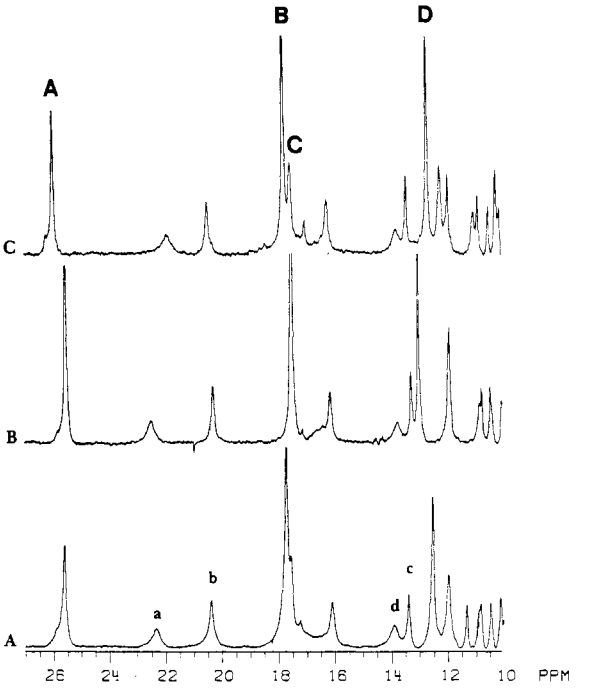

FIGURE 2: Downfield region of the three metMbCN spectra in 90% H_2O/10% ^2H_2O, pH 8.0, 40 °C. (A) Sperm whale; (B) horse; (C) dog. The exchangeable peaks considered here are labeled a–d in the sperm whale spectrum; previous notation is used (Cutnell et al., 1981). The intensity distortion is due to the profile of the Redfield excitation. Signals A, B, C, and D were assigned elsewhere (Sheard et al., 1970; Mayer et al., 1974) to the heme 5-CH_3, 1-CH_3, 2-α-vinyl, and 8-CH_3, respectively.

Rates of exchange can also be determined from the line width of the NMR resonance. The exchange contribution to the line width was computed by the slow-exchange expression

$$\tau^{-1} = \pi(\delta - \delta_0) \quad (7)$$

where δ and δ_0 are the observed line width and the line width in the absence of exchange, respectively.

Results

Assignment of Resonances. The 27–10 ppm region of the 360-MHz proton NMR spectra of sperm whale, horse, and dog metcyanomyoglobins is presented in parts A, B, and C of Figure 2, respectively. The spectra were recorded in 90% H_2O/10% ^2H_2O with a Redfield excitation (Redfield et al., 1975) so that the exchangeable protons are detected. The similarity between the three spectra is obvious; structurally sensitive characteristics such as chemical shift and line width

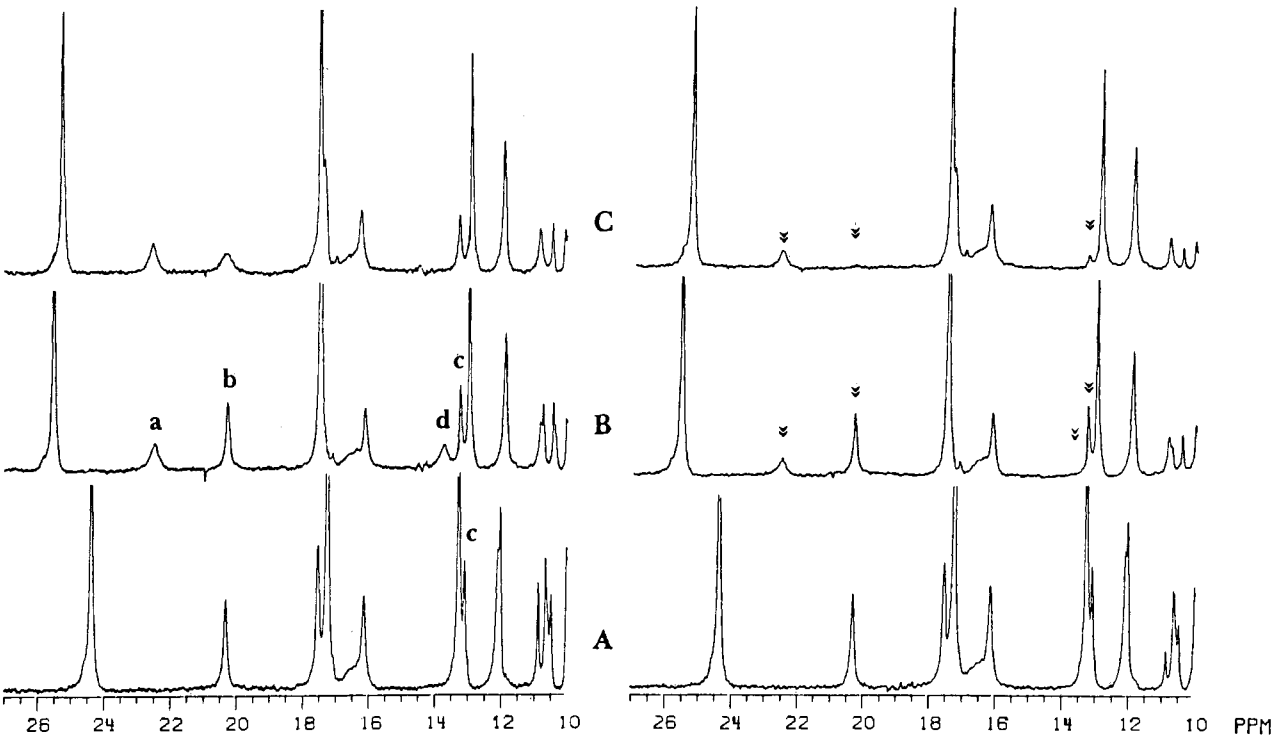

FIGURE 3: Saturation transfer pairs of spectra for horse metMbCN at 40 °C, 360 MHz. The traces on the left are the reference spectra (no water saturation) whereas the traces on the right were recorded with complete saturation of the H_2O line. (A) pH 5.2; (B) pH 8.03; (C) pH 9.97. Exchangeable peaks with $F < 1$ are marked on the right (double arrowheads).

Table I: Chemical Shifts of Assigned Hyperfine-Shifted Resonances of Various Metcyanomyoglobins in H_2O[a]

peak designation	sperm whale assignment	chemical shift		
		sperm whale	horse	dog
A	5-CH_3	25.58	25.51	25.94
a	H E7 ring NH	22.33	22.48	21.89
b	H F8 ring NH	20.35	22.48	20.43
B	1-CH_3	17.67	17.44	17.70
C	2-vinyl H_α	17.51	17.40	17.47
d	H FG3 ring NH[b]	13.89	13.72	13.73
c	H F8 peptide NH	13.36	13.24	13.37
E	8-CH_3	12.50	12.96	12.62
	I FG5 CH_3^γ	−3.00	−2.83	−2.97
	I FG5 CH_3^δ	−3.33	−3.23	−3.39
	I FG5 CH^γ	−8.28	−8.36	−8.47

[a] In parts per million relative to 2,2-dimethyl-2-silapentane-5-sulfonate (DSS) at 40 °C, pH 8.6. [b] Tentative assignment.

Table II: Nonselective Spin–Lattice Relaxation Times for Selected Protons in Metcyanomyoglobins[a]

proton[b]	pH	Mb[c]	T_1	
			40 °C	10 °C
E7 N_3H	9.2	SW	9.9	8.0
(a)		Eq		8.0
		Ca		7.8
F8 N_1H	9.2	SW		17.8
(b)		Eq		18.8
		Ca		19.8
F8 N_1H	4.7	SW	24.8	
(b)		Eq	27.4	
		Ca	24.9	
F8 NH	4.7	SW	114.0	
(c)		Eq	142.6	
		Ca	115.0	
5-CH_3		SW	86.3	59.0
(A)		Eq	92.0	58.0
		Ca	77.5[d]	66.0

[a] In milliseconds, for $F = 1$. [b] Peak labeling as in Figure 2. [c] SW, sperm whale; Eq (equine), horse; Ca (canine), dog. [d] Value shortened by off-acquisition saturation of the H_2O line.

are conserved for a large number of resonances. This observation is consistent with the fact that the heme cavities are highly homologous in terms of primary structure (Dayhoff, 1972). Hence, the assignments reported for the downfield hyperfine-shifted resonances of sperm whale metMbCN (Sheard et al., 1970; Mayer et al., 1974; Cutnell et al., 1981; La Mar & Krishnamoorthi, 1983) are applied to the corresponding signals in the spectra of the other two proteins; the relevant chemical shifts are listed in Table I. In particular, the 40 °C resonances at ~22.5 (labeled a in Figure 2A), ~20.5 (b), ~14 (d), and ~13.5 ppm (c) arising from four single exchangeable protons are attributed to the ring NHs of the distal histidine (E7), the proximal histidine, and tentatively histidine-97 (His FG3) and to the peptide NH of the proximal histidine, respectively (Sheard et al., 1970; Cutnell et al., 1981). Our study will focus on those four protons.

In metcyano-Mb, the nonselective spin–lattice relaxation data for hyperfine-shifted lines constitute useful structural information and provide a criterion for comparing the three proteins. Spin–lattice relaxation times were determined under several conditions of pH and temperature in ^2H_2O or 90% H_2O/10% ^2H_2O. T_1 values for the His F8 ring NH (b) and the peptide NH (c) peaks and a heme methyl (5-CH_3) peak are listed in Table II. Within experimental error, the heme methyl of horse and dog metMbCN, as well as the three exchangeable protons listed above, has T_1 values identical with those of the same protons or groups of protons in sperm whale metMbCN. Values for the distal His ring NH (a) were obtained at lower temperature (10 °C) in order to eliminate the chemical-exchange contribution and compare relaxation data corresponding to unity F factor; again, the same T_1 value holds for all three proteins (Table II).

Exchange Rates. In Figure 3, three pairs of spectra, at pH 5, 8, and 10, are presented for the horse protein. The reference traces, recorded without saturation of the H_2O resonance, are shown on the left, and the corresponding traces obtained with

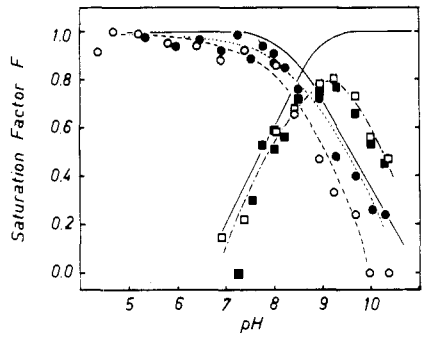

FIGURE 4: Plot of the saturation factor F vs. pH at 40 °C for horse and dog metMbCN. (○) Proximal His ring NH (b); (□) distal His ring NH (a). Open symbols and dashed lines represent horse data and closed symbols and dotted lines, dog data. The previously reported data for SWMbCN (Cutnell et al., 1981) are included for comparison as solid lines.

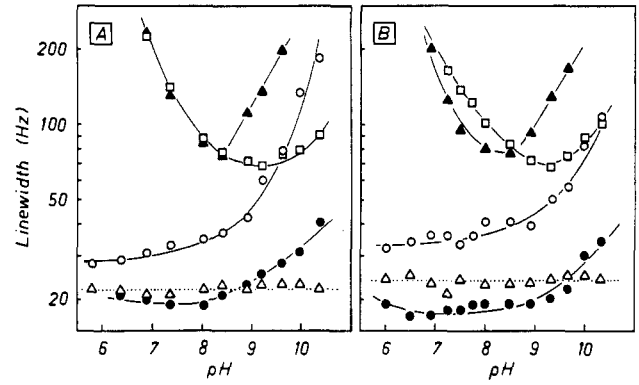

FIGURE 5: Plot of line width vs. pH at 40 °C for horse (A) and dog (B) metMbCN. (□) Distal ring NH (a); (○) proximal His ring NH (b); (●) proximal His peptide NH (c); (▲) His FG3 ring NH (d) (tentative); (△) 5-CH_3. The lines are meant to guide the eye.

complete H_2O saturation are displayed on the right. In both sets, the pulse sequence applied for observation did not perturb the water line significantly. Three of the four exchangeable protons considered in this study behaved in horse metMbCN (and dog metMbCN, not shown) as they do in sperm whale metMbCN (Cutnell et al., 1981). The proximal His ring NH (b) experiences increasing saturation upon H_2O irradiation as the pH is raised above 8, the ring NH d undergoes complete saturation at all pHs, and the proximal His peptide NH (c) behaves as the ring NH of the same residue.

Both horse and dog Mb, however, differ significantly from sperm whale Mb in the effect of pH on the saturation factor for the distal His E7 ring NH (a). As illustrated in spectrum A of Figure 3, there is efficient H^+ catalysis below pH 8 where the peak is broadened beyond detection by the exchange process. At pH 8 (spectrum B in Figure 3) the rate is slower: the peak is observed and exhibits some saturation transfer. At pH ~10, whereas in sperm whale metMbCN the rate of exchange is negligible with respect to ρ, OH^- catalysis is accelerating the reaction in the other two proteins and the saturation factor is measurable and less than unity.

Additional pairs of spectra, with no water excitation or off-acquisition saturation of the water line, were collected at several pHs, and the resulting saturation factors for His F8 ring NH (b) and His E7 ring NH (a) are plotted vs. pH in Figure 4. The dashed lines refer to the horse data, the dog data are represented by dotted lines, and to facilitate comparison, the profiles reported for the sperm whale Mb are included in solid lines; all lines are meant to guide the eye and do not represent the result of a theoretical fit. Both in the dog and in the horse protein, His E7 (a) displays a minimum of saturation transfer at pH ~9.2 that is not present in the sperm whale protein.

The line width of the NMR signals is also indicative of the rate of exchange: Figure 5 presents the line width variation as a function of pH. The four exchangeable NH peaks of horse metMbCN and dog metMbCN are represented as well as the heme 5-CH_3, which we use as a reference for the overall state of the pocket. The line width of His F8 ring NH (b) and peptide NH (c) parallels that of the 5-CH_3 up to pH 7. At higher pH, the 5-CH_3 line retains the same width whereas those of His F8 (peaks b and c) increase monotonically, reflecting lifetime broadening. On the other hand, the His E7 ring NH signal (a) becomes detectable at pH 7, sharpens until pH 9.2 is reached, and then broadens again, which is consistent with the saturation factor data of Figure 4 in combination with a constant ρ. The ring NH peak d is sharpest at pH 8.4, as previously observed in sperm whale metMbCN. Overall, the

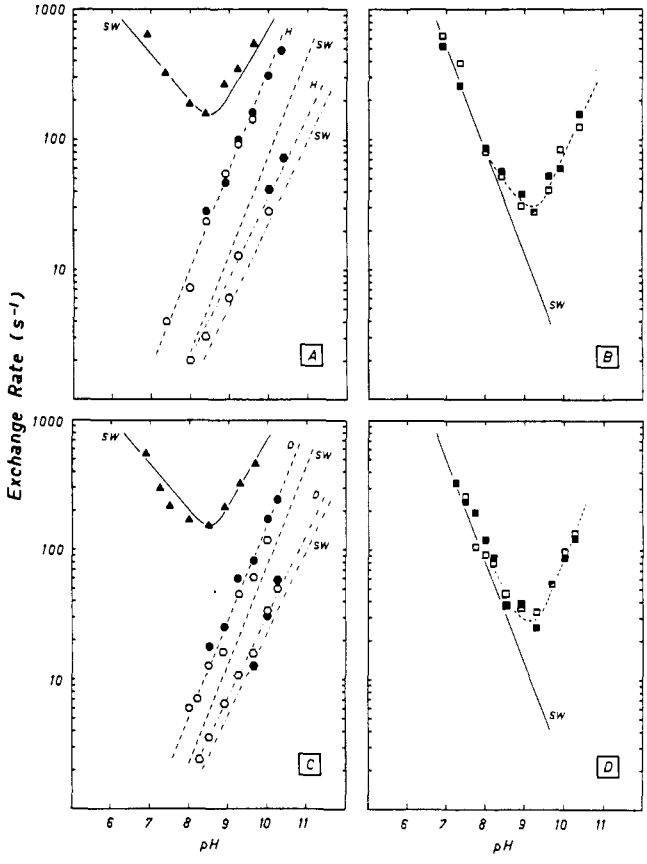

FIGURE 6: Plot of the logarithm of the rate of exchange vs. pH for four heme cavity protons in horse and dog metMbCN. (A) Horse proximal side: (○) proximal His ring NH (b); (○) proximal His peptide NH (c); (△) His FG3 ring NH (d) (tentative). (B) Horse distal side: (□) distal His ring NH (a). Open symbols represent points obtained from saturation transfer data and filled symbols, points obtained from line width data. The corresponding rate profiles for sperm whale metMbCN (Cutnell et al., 1981) are included and marked "SW". (C) Dog proximal side. (D) Dog distal side. In (C) and (D), the same conventions are used as in (A) and (B).

same characteristics are exhibited by the dog protein. It is interesting to note that the line width of the nonexchangeable protons is ca. 25% sharper in horse and dog metMbCN than in sperm whale metMbCN.

The values of the exchange rate τ_i^{-1} for the labile protons were extracted from the saturation transfer results combined with the relaxation parameters (listed in Table III) according to eq 4 and 5 and from the line width data by applying 7; they are plotted vs. pH in Figure 6. In the case of both horse and

Table III: Selective and Effective Spin–Lattice Relaxation Times for Selected Protons in Metcyanomyoglobins[a]

proton[b]	pH	Mb[c]	F	ρ^{-1} [d]	ρ'^{-1} [e]
E7 N_3H	9.2	SW	1.0	8.9	
(a)		Eq	0.9	8.8[f]	7.9
		Ca	0.8	9.1[f]	7.5
F8 N_1H	9.2	SW	0.7	24.7[f]	16.8
(b)		Eq	0.5	26.0[f]	12.2
		Ca	0.6	25.7[f]	14.9
F8 N_1H	4.7	SW	1.0	25.0	
(b)		Eq	1.0	22.2	
		Ca	1.0	25.3	
F8 NH	4.7	SW	1.0	50.2	
(c)		Eq	1.0	75.3	
		Ca	1.0	68.9	

[a] In milliseconds, at 40 °C. [b] Peak labeling as in Figure 2. [c] Metcyanomyoglobin: SW, sperm whale; Eq, horse; Ca, dog. [d] Selective value. [e] Effective value. [f] Calculated by using eq 6.

dog metMbCN, the ρ value of the His E7 ring NH (a) could not be obtained by direct method since at 40 °C and all pH values the exchange takes place with a competing rate ($F < 1$). However, the number extracted from the ρ' data, in combination with eq 5 and 6, yields an estimate of τ^{-1} and ρ. The line width of the ring NH resonance d in the absence of exchange was estimated from the sperm whale data (Cutnell et al., 1981), taking into account the general line sharpening observed in the two homologues.

For protons on the proximal side of the heme (peaks b, c, and tentatively d), the rates of exchange as a function of pH in horse and dog metMbCN are compared with the previous data for sperm whale metMbCN in panels A and C of Figure 6. For peak d, the rate data in the three proteins are practically superimposable; thus acid- and base-catalyzed exchange must be the same for each of the three proteins. Similarly, the rates of (base-catalyzed) exchange for peak c (His F8 peptide NH) are almost indistinguishable among the three proteins. For peak b (His F8 ring NH), the experimental data for horse and dog metMbCN fall on a straight line which is parallel, within experimental error, to that for the same peak in sperm whale metMbCN. Thus, the identical mechanism (base catalysis) is operative but with small differences in the magnitudes for the three proteins; the rate data are collected in Table IV.

In contrast to the very similar catalytic mechanisms observed for the proximal side residues in the three proteins, the ring NH of the distal His E7 (peak a) exhibits a significant difference. The rate data as a function of pH for horse and dog metMbCN are illustrated in panels B and D of Figure 6, respectively; in each case the data are compared to the previous results on sperm whale metMbCN, reproduced as a solid line. The rate data are essentially the same for the three proteins in the low pH region; hence, acid catalysis does not differentiate among the three proteins. Both horse and dog metMbCN, however, exhibit significant base-catalyzed exchange at alkaline pH; sperm whale metMbCN has a unity saturation factor above pH 9, which dictates that, at the highest pH reached in the experiment (10.5), $\tau_a^{-1} < 10\ s^{-1} \sim 0.1\rho_a$. The exchange rates for base catalysis in the dog and horse proteins are measurable and are compared in Table IV.

Discussion

Structure of the Heme Pocket. The ^{1}H NMR characteristics of hyperfine-shifted resonances in heme proteins are known to depend strongly upon the interactions between the heme moiety and the protein core (La Mar, 1979). In particular, the spin–lattice relaxation rates and chemical shifts are sensitive indicators of the heme pocket geometry, and they provide effective probes for comparing the three myoglobins. Table II illustrates that at 40 °C and acidic pH the nonselective relaxation time T_1 for the His F8 ring NH (b) has very similar values in horse, dog, and sperm whale Mb, yielding, in accordance with eq 2, an $r(b)/r(CH_3) \sim 0.8$, which agrees well with the X-ray ratio of 0.81 (Cutnell et al., 1981). At acidic pH and 40 °C, the His E7 ring NH of sperm whale metMbCN undergoes a slow chemical exchange compared to its ρ ($F = 1$), permitting direct measurement of T_1. However, under the same conditions, the same proton in horse and dog Mb has exchange rates comparable to ρ so that the nonselective T_1 values is not interpretable at 40 °C. By lowering the temperature to 10 °C at the pH where the exchange is the slowest (pH 9.2), a true nonselective value can be recorded (Table II).[2] The ratio $r(a)/r(CH_3)$, as determined by eq 2, is ~0.7 in all three proteins and thus indicates that the 4.2-Å distance of the distal ring NH to the Fe atom is conserved.

The hyperfine-shift pattern for heme methyls, due mainly to the contact interaction, is quite sensitive to the orientation of the proximal histidine with respect to the heme plane (La Mar, 1979); the nearly identical heme methyl (and vinyl) shifts for the three proteins (Table I) point to unaltered proximal histidine interaction with the heme. For the distal His E7 ring NH (and also for the Ile FG5 γ-CH, γ'-CH, and δ-CH_3), the hyperfine interaction is dipolar in origin (Ramaprasad et al., 1984) and depends on angular variables as well as the inverse cube of the distance to the iron. As seen in Table I, the observed shifts for all of these resonances are essentially the same, implying (particularly for the His E7 ring NH) that since r is the same from relaxation data, even the angular variables differ inconsequentially for the functional groups in the heme cavity. We therefore conclude that both the proximal and the distal histidines, as well as nonbonded amino acid side chains (Ile FG5), have comparable orientations and interactions in the three proteins of interest. Thus we can detect no significant differences in the ground-state structure of the heme pocket for the metcyano complexes of sperm whale, horse, and dog Mb. In particular, the interaction between the distal histidine and the iron-bound cyanide ligand appears indistinguishable in the three complexes. In the absence of a structural basis for interpreting the difference in exchange behavior of the distal histidine ring NH, we turn to the dynamic properties of the heme pocket.

Exchange Mechanism. The observation of clear pH influences on the exchange rates that mimic (at least for d and His F8) the pH-dependent characteristics of the exposed group indicates that the EX_2 mechanism is an acceptable model for describing the exchange behavior (Woodward et al., 1982). In this model the observed rate is expressed as

$$\tau_i^{-1} = K_{op}^{B}(i)k_B[OH^-]^m \quad \text{(for base catalysis)} \qquad (8)$$

$$\tau_i^{-1} = K_{op}^{A}(i)k_A[H^+]^n \quad \text{(for acid catalysis)} \qquad (9)$$

where $K_{op}^{A,B}(i)$ are the equilibrium constants for the opening of the channels (or the locally unfolded state) allowing H^+ or OH^-, respectively, to reach proton i. The local unfolding model predicts equal K_{op}^{A} and K_{op}^{B} for the histidine ring. On the other hand, these equilibrium constants can differ in the penetration

[2] It appears that there is no difference between nonselective (Table II) and selective (Table III) T_1 values (within experimental error) for the proximal and distal His ring NHs (a and b), an observation reflecting the dominance of the paramagnetic contribution and the relatively small participation of cross-relaxation effects. Selective and nonselective values are expected to differ for protons located further away from the paramagnetic center. Such is the case for the His F8 peptide NH (c) which is found at $r > 6.2$ Å from the iron.

Table IV: Exchange Rates τ^{-1} and Relative Equilibrium Constants K_{op} for Labile Histidine Protons in the Heme Cavity of Metcyanomyoglobin[a]

	proximal side histidine proton[b]				distal side histidine proton	
	FG3 ring NH (d)	FG3 ring NH (d)	F8 peptide NH (c)	F8 ring NH (b)	E7 ring NH (a)	E7 ring NH (a)
exchange catalyst	acid	base	base	base	acid	base
pH	6.5	10.0	10.0	10.0	7.0	10.0
τ^{-1} (sperm whale)	7×10^2	7×10^2	23	80	5×10^2	<10
K_{op} (SW:H:D)[c]	1:1:1	1:1:1	1:1.5:1.5	1:4:2	1:1:1	1:32:33

[a] $\tau_X^{-1} = K_{op}k_X[X]^n$ in s^{-1} at 40 °C. [b] The FG3 assignment is tentative. [c] Ratio of τ^{-1}, normalized to sperm whale: SW, sperm whale; H, horse; D, dog.

model since they depend upon the orientation of the side chains with respect to the channels. The rate constants k_A and k_B are assumed to be the same as in model compounds or denatured proteins and, more importantly, the same for a given proton in each of the three proteins being considered. Thus, the difference in τ^{-1} for the same protons exhibiting the same exchange mechanism yields directly the difference in K_{op} in the various proteins. The corresponding free energy of the state in which the proton i is exposed is expressed by

$$\Delta G_{op} = -RT \ln K_{op}(i) \qquad (10)$$

For the three protons on the proximal side of the heme, there is qualitative agreement in the pH profiles of the three proteins; the comparative rate data provided in Table IV show it is likely that the exchange proceeds in the same fashion. Indeed, the traces obtained for the His F8 peptide NH (c) and the presumed His FG3 ring NH (d) are practically superimposable at all pHs and impose similar K_{op} for c and d in the three proteins. The rates for the proximal His ring NH (b) are essentially parallel, with τ^{-1} slightly faster in horse and dog Mb (Figure 6), which yields small differences in K_{op}(a), as given in Table IV.

In contrast, on the distal side of the heme, the identical τ^{-1} values for peak a at acidic pH dictate the same K_{op}^A, while at alkaline pH, K_{op}^B (horse) or K_{op}^B (dog) are much larger than that for sperm whale metMbCN. At extremely high pH (11.0) at 40 °C, the base-catalyzed exchange rate for sperm whale metMbCN is less than $0.1\rho \sim 10\ s^{-1}$; under the same conditions the rates are 320–330 s^{-1} for the horse and dog proteins. Thus K_{op}^B(b) must differ by a factor ≥30 (Table IV).

The difference in the sensitivity of the base catalysis and the insensitivity of the acid catalysis for the ring NH exchange of the distal His E7 can be rationalized in terms of a rapid equilibrium involving the formation of a ligation channel as described below.

The Distal Histidine Trap Door. We propose here a model for interpreting the peculiar distal side exchange behavior in the proteins of interest and use to this end the dynamics of that portion of the molecule. First, the efficient and invariant acid-catalyzed exchange of the ring NH of His E7 indicates that protons have access to this portion of the heme cavity to the same degree in the three proteins. Second, the attack of hydroxyl ions is precluded when His E7 is enclosed in the environment provided by sperm whale myoglobin but leads to much faster exchange in the horse and dog proteins. This can be described by an equilibrium between the X-ray structure of metMbH_2O (Figure 1A) and that of the novel σ-phenyl-ligated metMb complex (Ringe et al., 1984) which has its "door" stuck open (Figure 1B). We assume that the histidine ring orientation as in Figure 1A constitutes the "closed" door with respect to access of hydroxyl ions to the ring NH involved in the hydrogen bond with the coordinated cyanide (i.e., acid but not base catalysis). On the other hand, the "open" orientation, as in Figure 1B, would freely allow OH^--catalyzed exchange as in a free histidine (comparable acid and base catalyses).

When comparing the rate data for His E7 in the basic range, we concluded because of the accelerated τ^{-1} that K_{op}^B(b) is at least 30 times larger in horse and dog metMbCN than in sperm whale metMbCN. K_{op}^B(b), the equilibrium constant for the channel opening, represents the probability of the B ring orientation relative to that of the A ring orientation in Figure 1; that is, it reflects the degree to which the last "door" to the ring NH is open. Therefore, the relative rates indicate that B is at least 30 times more probable in horse or dog Mb than in sperm whale Mb. Considerably less side-chain motion is involved to allow protons access to the ring N_1; hence a similar K_{op} is not unreasonable for the three proteins.

This factor of ~30 between the K_{op}^B values in the proteins of interest translates into a stabilization of the open door (Figure 1B) greater by 2.1 kcal/mol (ΔG) in horse or dog Mb than in sperm whale Mb. The values of K_{op}^B are not determinable for either protein, but assuming diffusion-controlled base catalysis, as observed for a free imidazole ring ($k_B \sim 10^{10}$ s^{-1}; Eigen, 1964) and taking the measured rate for horse Mb equal to 3×10^2 at pH ~11, we estimate $K_{op}^B \sim 3 \times 10^{-5}$ for horse and dog Mb and thus $K_{op}^B \sim 10^{-6}$ for sperm whale Mb. While the relative values for the three proteins are well-defined, the absolute values are only estimates but serve to support the fact that the "open" door is an event of sufficiently low probability (even in horse MbCN) so as to be undetectable in the time-average NMR spectral parameters that we have used to describe the ground-state structure. Furthermore, in the EX_2 case, the rate of exposure is not limiting, and if K_{op} is represented by k_{op}/k_{cl} (k_{op} and k_{cl} are the rates for the opening and the closing of the channel), it must be faster than k_B, that is, faster than $10^7\ s^{-1}$. The open–closed fluctuations of the protein matrix occur therefore with a high frequency.

The structural basis for the significant difference in the stability of the open channel to the His E7 ring NH in the myoglobins studied here can be traced to one amino acid substitution common to both horse and dog Mb in the distal heme pocket: CD3 Arg (sperm whale) → Lys (horse, dog) (Dayhoff, 1972).[3] Arg CD3 plays a crucial role in stabilizing the structure of the heme pocket and is one of only four residues whose side-chain orientation is altered upon opening the ligand channel in σ-phenyl-ligated sperm whale metMb (Ringe et al., 1984). In sperm whale Mb, the guanidyl group of Arg CD3 forms hydrogen bonds to both the carboxylate of Asp E3 and that of the heme 6-propionate (Takano, 1977a,b), thereby stabilizing the histidine orientation as depicted in Figure 1A. In horse and dog Mb, the Lys that replaces Arg, with its shorter side chain unable to form simultaneous hydrogen bonds to the same two residues, does not stabilize to the same extent the histidine orientation of Figure 1A. The hydrogen bonds of Arg CD3 are both ruptured in opening the ligand channel in σ-phenyl-ligated sperm whale metMb (Ringe et al., 1984).

[3] Horse Mb has another amino acid substitution with respect to sperm whale (Thr E10 → Val E10). It cannot be responsible for the effects we observe as the dog Mb does not present that replacement.

While this model is merely our rationalization for a significantly enhanced base-catalyzed His E7 ring NH exchange in horse and dog Mb, it does provide the basis for interpreting the reported observation that while the ligand affinities for a variety of alkyl isocyanides are the same in sperm whale and horse Mb, both the ligand on-rates and ligand off-rates are consistently larger in the latter protein (Stetzkowski et al., 1979).

The considerably smaller difference in rates (with identical mechanisms) for protons on the proximal side of the heme suggests that the structural fluctuations that allow OH^- access to the coordinated ring of His F8 vary slightly in the three proteins. The characterization of the transient channels for the proximal side process is more difficult since no amino acid substitution can be directly invoked. It may be noted, however, that the slight increase of horse (a factor of 5) and dog (a factor of 6) rates over sperm whale rates parallels the trend in the overall folding free energy of the three proteins (Puet, 1973; McLendon, 1977) and hence may reflect a small general increase in protein flexibility with decreasing $\Delta G_{\text{folding}}$.

We therefore conclude that the exchange rate of labile protons of histidine side chains provides a valuable probe of the nature of solvent-accessible states in the heme cavity of hemoproteins. The mechanisms and relative rates of exchange of labile protons in the heme cavity of Mb support a dynamic equilibrium between a closed Mb pocket and an open channel for which the distal histidine side chain rotates away from its position close to the ligand-binding side. The greater relative stability of the open channel for horse Mb compared to that of sperm whale Mb can be used to rationalize the faster ligation rates observed in the former protein.

Future work in this laboratory aimed at assigning resonances and designing better dynamic probes to detect differential side-chain mobility in horse and sperm whale Mb may provide additional information on the nature of protein motions allowing solvent access into the protein interior.

ACKNOWLEDGMENTS

The use of the facilities of the University of California—San Francisco Computer Graphics Laboratory is gratefully acknowledged.

Registry No. Heme, 14875-96-8.

REFERENCES

Bretscher, P. A. (1968) Ph.D. Thesis, Cambridge University, Cambridge, England.

Campbell, I. D., Dobson, C. M., Ratcliffe, R. G., & Williams, R. J. P. (1978) *J. Magn. Reson. 29*, 397–417.

Case, D. A., & Karplus, M. (1979) *J. Mol. Biol. 132*, 343–368.

Cutnell, J. D., La Mar, G. N., & Kong, S. B. (1981) *J. Am. Chem. Soc. 103*, 3567–3572.

Dayhoff, M. O. (1972) *Atlas of Protein Sequence and Structure*, Vol. 5, National Biomedical Research Foundation, Washington, DC.

Debrunner, P. G., & Frauenfelder, H. (1982) *Annu. Rev. Phys. Chem. 33*, 283–299.

Eigen, M. (1964) *Angew. Chem., Int. Ed. Engl. 3*, 1–72.

Englander, S. W. (1975) *Ann. N.Y. Acad. Sci. 244*, 10–27.

Gurd, F. R. N., & Rothgeb, T. M. (1979) *Adv. Protein Chem. 33*, 73–165.

Hvidt, A., & Nielsen, S. (1966) *Adv. Protein Chem. 21*, 287–386.

Karplus, M., & McCammon, J. A. (1981) *CRC Crit. Rev. Biochem. 9*, 293–349.

La Mar, G. N. (1979) in *Biological Applications of Magnetic Resonance* (Shulman, R. G., Ed.) pp 305–343, Academic Press, New York.

La Mar, G. N., & Krishnamoorthi, R. (1983) *Biophys. J. 44*, 177–183.

Levitt, M. H. (1982) *J. Magn. Reson. 48*, 234–264.

Mayer, A., Ogawa, S., Shulman, R. G., Yamane, T., Cavaleiro, J. A. S., Rocha-Gonsalves, A. M. d'A., Kenner, G. W., & Smith, K. M. (1974) *J. Mol. Biol. 86*, 749–756.

McCammon, J. A. (1984) *Rep. Prog. Phys. 47*, 1–84.

McCammon, J. A., & Karplus, M. (1980) *Annu. Rev. Phys. Chem. 31*, 29–45.

McCammon, J. A., & Karplus, M. (1983) *Acc. Chem. Res. 16*, 187–193.

McLendon, G. (1977) *Biochem. Biophys. Res. Commun. 77*, 959–966.

Nobbs, C. D. (1966) in *Hemes and Hemoproteins* (Chance, B., Eastbrook, R. W., & Yonetani, T., Eds.) pp 143–147, Academic Press, New York.

Perrin, C. L., & Arrhenius, G. (1982) *J. Am. Chem. Soc. 104*, 6693–6696.

Perutz, M. F. (1976) *Br. Med. Bull. 32*, 195–208.

Perutz, M. F., & Mathews, F. S. (1966) *J. Mol. Biol. 21*, 199–202.

Phillips, S. E. V. (1980) *J. Mol. Biol. 142*, 531–534.

Phillips, S. E. V., & Schoenborn, B. P. (1981) *Nature (London) 292*, 81–82.

Puet, D. J. (1973) *J. Biol. Chem. 248*, 4623–4634.

Ramaprasad, S., Johnson, R. D., & La Mar, G. N. (1984) *J. Am. Chem. Soc. 106*, 5330–5335.

Redfield, A. G., Kunz, S. D., & Ralph, E. K. (1975) *J. Magn. Reson. 19*, 114–117.

Ringe, D., Petsko, G. A., Kerr, D. E., & Ortiz de Montellano, P. R. (1984) *Biochemistry 23*, 2–4.

Sheard, B., Yamane, T., & Shulman, R. G. (1970) *J. Mol. Biol. 53*, 35–48.

Stetzkowski, F., Cassoly, R., & Banerjee, R. (1979) *J. Biol. Chem. 254*, 11351–11356.

Swift, T. J. (1973) in *NMR of Paramagentic Molecules* (La Mar, G. N., Horrocks, W. D., Jr., & Holm, R. H., Eds.) pp 53–83, Academic Press, New York.

Takano, T. (1977a) *J. Mol. Biol. 110*, 537–568.

Takano, T. (1977b) *J. Mol. Biol. 110*, 569–584.

Tuchsen, E., & Woodward, C. K. (1985) *J. Mol. Biol. 185*, 421–430.

Unger, S. W., Jue, T., & La Mar, G. N. (1985) *J. Magn. Reson. 61*, 448–456.

Vold, R. L., Waugh, J. S., Klein, M. P., & Phelps, D. E. (1968) *J. Chem. Phys. 48*, 3831–3832.

Woodward, C. K., & Hilton, B. D. (1979) *Annu. Rev. Biophys. Bioeng. 8*, 99–127.

Woodward, C., Simon, E., & Tuchsen, E. (1982) *Mol. Cell. Biochem. 48*, 135–160.